Structural Analysis of the NH₃-dependent NAD⁺ Synthetase from *Deinococcus radiodurans*

Young Woo Park, Hyun Ku Yeo, and Jae Young Lee[*]

*Department of Life Science, Dongguk University, Seoul 100-715, Korea. *E-mail: jylee001@dongguk.edu*

Nicotinamide adenine dinucleotide (NAD) is a ubiquitous molecule involved in both redox reactions as a cofactor and numerous regulatory processes as a substrate such as cell cycle, calcium signaling, immune response, and DNA repair.[1] The biosynthesis of NAD⁺ is vitally important in all living organisms and has been studied extensively in variety of species for antibiotic drug development.[2] The NAD⁺ is synthesized through two metabolic processes which are de novo and salvage pathways.[3] Despite some variations in the early steps of two pathways, the final step of NAD⁺ synthesis from nicotinic acid adenine dinucleotide (NaAD) to NAD⁺ is highly conserved. NAD⁺ synthetase (NADS, EC. 6.3.5.1) catalyzes conversion of NaAD to NAD⁺ through two steps; first step is the adenylation of NaAD in the presence of ATP and Mg^{2+}; second, the NAD-adenylate intermediate is attacked by nucleophilic ammonia leading to generate NAD⁺ and AMP (Fig. 1(a)).[4] The NADS family is categorized into two subgroups: (i) NH₃-dependent NADS present only in prokaryotes, which has only synthetase domain (S-domain), and (ii) glutamine-dependent NADS present in all eukaryotes and some prokaryotes, which has an additional glutamine amide transfer domain (GAT-domain).

The crystal structures of NH₃-depenent NADS from bacterial species including *Bacillus subtilis* (*bsu*NADS), *Escherichia coli* (*eco*NADS), *Bacillus anthracis* (*ban*NADS), *Helicobacter pylori* (*hpy*NADS), and *Francisella tularensis* (*ftu*NADS) have been determined.[5-9] As the prokaryotic and eukaryotic NADS differ in size, enzymatic activity and substrate requirements, NADS is an attractive target for the development of a new class of antibiotics. The NADS homolog (UniProt code Q9RYV5) in *Deinococcus radiodurans* encodes a protein of 287 amino acid residues, with 59% sequence identity to that of *E. coli*. Further sequence comparisons of *D. radiodurans* NADS (*dra*NADS) with *bsu*NADS, *ban*NADS, and *ftu*NADS shows 58%, 59%, and 36% sequence identity, respectively (Fig. 2(a)). In order to obtain structural and functional information of *dra*NADS protein, we report here the crystal structure of NH₃-dependent NADS homolog from *D. radiodurans* at 2.60 Å resolution.

Materials and Methods

Protein Expression and Purification. The *nadE* gene encoding NADS was amplified by polymerase chain reac-

tion using genomic DNA of *D. radiodurans* as a template. It was inserted into the NdeI/BamHI-digested expression vector pET-28b(+) (Novagen), resulting in a twenty-residue hexahistidine-containing tag at its N-terminus. The recombinant *dra*NADS was expressed in *E. coli* BL21 (DE3) star pLysS cells (Invitrogen). Overexpression of the recombinant protein was induced with 1.0 mM isopropyl β-D-thiogalacto-pyranoside (IPTG) and the cells were continuously cultured at 303 K for 4 h. After harvest of the cells by centrifugation at 4200 g for 10 minutes at 277 K, the pellet was re-suspended in a lysis buffer [20 mM Tris-HCl (pH 8.0), 0.5 M NaCl, 10% glycerol, 1 mM phenylmethylsulfonyl fluoride] and homogenized by an ultrasonic processor. The insoluble fraction was removed by centrifugation at 31000 g for 60 minutes at 277 K and the recombinant *dra*NADS in the supernatant fraction was purified by three chromatographic steps. The first step was a metal-chelate chromatography on Ni-NTA resin (GE Healthcare). The His-tagged *dra*NADS protein was eluted with buffer A (20 mM Tris-HCl at pH 8.0, 0.5 M NaCl, 10% glycerol) containing 300 mM imidazole followed by enzymatic removal of the His-tag by overnight incubation with prescission protease. The uncleaved His-tagged protein and prescission protease were removed from the target *dra*NADS applying to Ni-NTA affinity column. The next step was gel filtration on a Super-dex-75 column (GE Healthcare), employing an elution buffer of 0.2 M NaCl, 20 mM Tris-HCl at pH 8.0, 1 mM DTT, 5 mM MgCl₂ and 5% glycerol. The purified protein was concentrated to 30 mg/mL using Centricon YM-10 (Milli-pore) and aliquots of the protein were stored at 193 K.

Crystallization and Data Collection. Initial crystalli-zation was performed by the sitting-drop vapor diffusion method using 96-well CrystalQuick plates (Greiner Bio-One) and commercial screens (Hampton Research; Qiagen; Emerald Biosystems) at 296 K. Crystals of the *dra*NADS were initially grown in several conditions containing poly-ethylene glycol (PEG) 4000 and lithium sulfate, which were further optimized to 20% PEG 4000, 0.2 M lithium sulfate, 0.1 M MES at pH 6.0. The crystals grew reproducibly up to approximately 0.1 × 0.2 × 0.05 mm within 3 days. Crystals were transferred into a cryoprotectant solution containing 20% glycerol in reservoir solution and then flash-cooled in liquid nitrogen. X-ray diffraction data were collected to 2.6 Å at 100 K using an ADSC Quantum 210 CCD image-plate

detector on Beamline SB-I of the Pohang Accelerator Laboratory, Korea. The crystals belonged to the orthorhombic space group $P2_12_12_1$, with unit cell parameters of a = 113.23 Å, b = 114.15 Å, and c = 121.62 Å. Two *dra*NADS dimers were present in an asymmetric unit, giving a solvent fraction of 61.1%. All data were processed and scaled with iMOSFLM program suite.[4,10]

Structure Determination and Refinement. The *dra*NADS crystal structure was solved by molecular replacement using program PHASER[11] using the *ban*NADS coordinates (PDB code 2PZ8)[7] as a search model. Subsequently, the initial model was further improved by the alternating cycles of manual building using the COOT program[12] and the model was refined with the PHENIX program.[13] The refined model was evaluated using MolProbity.[14] X-ray data collection and refinement statistics are presented in Table 1. The coordinate and structure factor have been deposited in the Protein Data Bank under accession number 4Q16.

Result and Discussion

The crystal structure of *dra*NADS was determined by molecular replacement at 2.60 Å resolution. The structure was refined to crystallographic R_{work} and R_{free} values of 23.9% and 29.2%, respectively. The refined model (PDB code 4Q16) contained 1,064 residues of the two independent *dra*NADS dimers, 8 molecules of sulfate ion, and 362 water molecules in the asymmetric unit. In each subunit, an internal region of the polypeptide chain (Glu221–Arg224 in subunit A, Val215–Glu221 in subunit B, Arg213–Pro228 in subunit C, and Asp219–Asp222 in subunit D) and terminal residues (Met1–Pro7 and Gly282–Ser287 in subunit A, Met1–Leu6 and Gly282–Ser287 in subunit B, Met1–Pro10 and Gly282–Ser287 in subunit C, and Met1–Pro7 and Glu283–Ser287 in subunit D) were disordered. Each *dra*NADS subunit has single α/β core domain consisting of 4 parallel β-stands, 11 α-helices and connecting loops, which shows typical Rossman fold. The core domains of the two subunits are formed homodimer, with approximate dimensions of 42 Å × 53 Å × 65 Å (Fig. 1(b)). The solvent accessible surface area buried at the interface in the dimeric unit is about 2556 Å² (19% of their individual accessible surface areas). The extended C-terminal loops (residues 266-276) and the α-helix bundle (residues 116-159) composed of
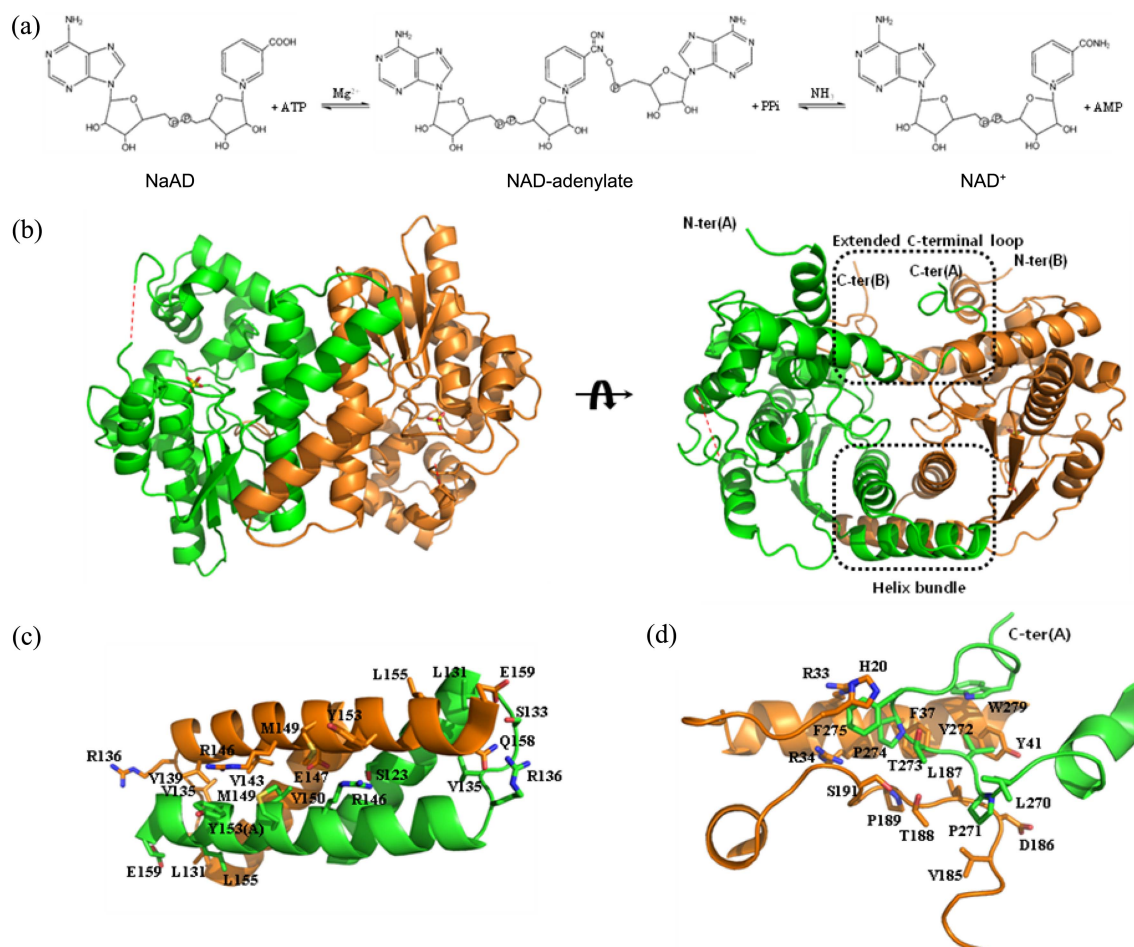
Figure 1. Overview of NAD⁺ synthetase from *D. radiodurans.* (a) A scheme of the reaction catalyzed by NAD⁺ synthetase. (b) Overall structure of *dra*NADS homodimer. Each subunit is colored by green and orange, respectively. The red dotted line indicates the long flexible loop (residues 213-235). The helix bundle and extended C-terminal loops are indicated by dotted boxes. The sulfate ions are shown as the ball-and-stick. Close up view of the helix bundle (c) and the extended C-terminal loop (d). The figures (c) and (d) are reoriented for clarity. The residues involved in dimeric interface are drawn as ball-and-stick.
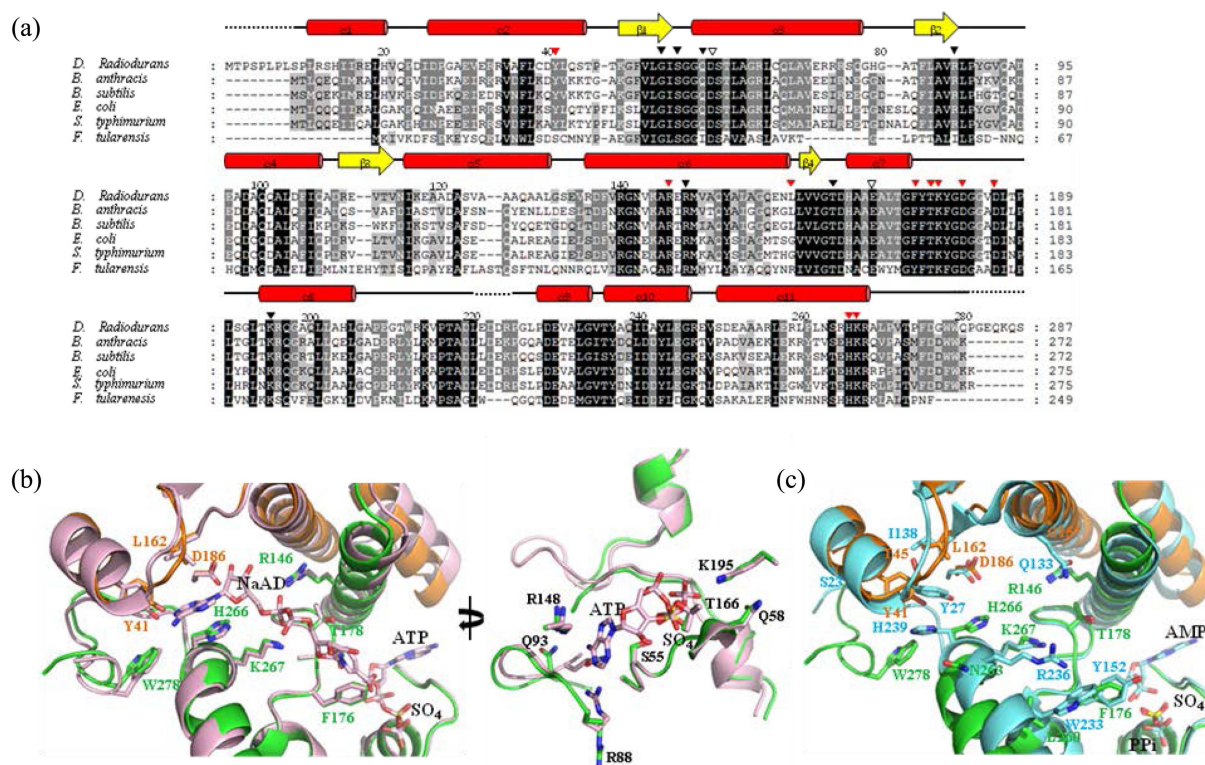
Figure 2. Structural and sequence analysis of *dra*NADS with the other homologous NADS proteins. (a) Multiple sequence alignment of *dra*NADS and the represented homologous NADS proteins (*B. anthracis, B. subtilis, E. coli, S. typhimurium and F. tularensis*). The highly conserved residues involved in NaAD, ATP and Mg^{2+} binding are indicated as red closed triangles, black closed triangles and open triangles, respectively. (b) Superposition of *dra*NADS (subunit A: green, subunit B: orange) and *bsu*NADS-NaAD-ATP complex (PDB code 2NSY, pink) shows a detailed view of the substrates binding sites. ATP binding pocket was shown by 90° rotation from the left panel. (c) Superposition of *dra*NADS and *ftu*NADS-AMP-PPi complex (cyan) shows detailed view of NaAD binding pockets. The substrate binding residues from *dra*NADS subunits (A, B) and *ftu*NADS are shown in green, orange, and cyan, respectively.

two helices mainly participate in dimerization (Fig. 1(c)). Especially, the C-terminal segment and helix-loop motif (residues 116-136) are similar to arms of clamp and anchor the subunits to each other (Fig. 1(d)). The dimeric interface is predominantly contributed by both hydrophobic interactions and hydrogen bonds.

The structural comparisons showed that the *dra*NADS structure is highly similar with other NH_3-depenent NADS structures, (i) *bsu*NADS (PDB code 2NSY, r.m.s. deviation of 1.0 Å for 267 equivalent Cα positions in residues 11-280 of *dra*NADS, a Z-score of 39.8, and a sequence identity of 58%),[5] (ii) *ban*NADS (PDB code 2PZ8, r.m.s. deviation of 1.1 Å for 269 equivalent Cα positions in residues 10-281 of *dra*NADS, a Z-score of 39.6, and a sequence identity of 59%),[7] (iii) *eco*NADS (PDB code 1WXI, r.m.s. deviation of 1.1 Å for 258 equivalent Cα positions in residues 11-281 of *dra*NADS, a Z-score of 36.7, and a sequence identity of 59%),[6] and (iv) *ftu*NADS (PDB code 3FIU, r.m.s. deviation of 1.6 Å for 234 equivalent Cα positions in residues 25-272 of *dra*NADS, a Z-score of 30.0, and a sequence identity of 36%)[9] (Fig. 2(a)).

Although the general NH_3-depenent NADS proteins from bacterial species have a substrate preference for NaAD, the *ftu*NADS mainly catalyzes from nicotinic acid mononucleotide (NaMN) to nicotinamide mononucleotide (NMN) different from general NADS enzymes. Multiple sequence alignment and structural superposition results showed that the substrate binding site of the apo *dra*NADS structure is well accommodate with NaAD. When the apo *dra*NADS structure is superimposed with *bsu*NADS-NaAD complex structure, the conformation of its residues involved in substrates binding site is almost identical with *bsu*NADS-NaAD complex structure (Fig. 2(b)). However, the conformation of *ftu*NADS substrate binding site is a little different. The Tyr41, Gly157, Leu260 and Asn263 residues in the *dra*NADS located at the NaAD binding pocket were replaced with Ser23, Gln133, Trp233 and Arg236 in *ftu*NADS. In particular, the conserved His266 residue which enabled to bind NaAD in *dra*NADS was oriented in the opposite direction in *ftu*NADS structure. The orientation of the His266 makes it possible for the NaAD to access into the binding pocket because the residue can avoid a crash with the adenosyl group of NaAD. While the corresponding residue His239 in *ftu*NADS was stabilized by a hydrogen bond and a stacking interaction with Tyr27, the same orientation of His266 would be blocked by the side chain of Trp278 which is missing in *ftu*NADS but highly conserved in other NADS proteins (Fig. 2).

Table 1. Data collection and refinement statistics

Data collection statistics	
Wavelength (Å)	0.97933
Resolution range (Å)	50.72–2.60 (2.64-2.60)
Number of observations	427798
Unique reflections	49185
Space group	$P2_12_12_1$
Unit-cell parameters (Å, °)	$a = 113.2$, $b = 114.2$, $c = 121.6$
Data completeness (%)	100 (99.9)
Redundancy	8.7 (7.3)
Average $I/\sigma(I)$	14.6 (4.4)
R_{merge} (%)^a	9.6 (37.6)
Refinement statistics	
Resolution (Å)	29.38-2.60
Reflections in working set	46018
Reflections in test set	2460
R_{work}/R_{free} (%)^b	23.91/29.28
r.m.s.d. bonds (Å)	0.002
r.m.s.d. angles (°)	0.539
Ramachandran plot (%)	
Favored	95.23
allowed	4.77

^{a}$R_{merge} = \Sigma h\ \Sigma i |$ I $(h,i) - <$ I $(h)> | /\Sigma h\ \Sigma i$I (h,i), where I (h,i) is the intensity of the i th measurement of reflection h and $<$ I (h) is the mean value of I (h,i) for all i measurements. ^{b}$R_{work} = \Sigma ||F_{obs}| - |F_{calc}|| / \Sigma |F_{obs}|$, where F_{obs} and F_{calc} are the observed and calculated structure-factor amplitudes, respectively. R_{free} was calculated as R_{work} using a randomly selected subset of ~5% of the unique reflections not used for structure refinement. Values in parentheses refer to the highest resolution shell.

In summary, we determined the NH_3-dependent *dra*NADS in apo form and analyzed the substrate binding sites of NaAD and ATP. The structure revealed a compact homo-dimer with an extended dimeric interface mediated by mainly the two pairs of helices α5 and α6. Similarities in the overall structure and the location of the substrate binding site residues of *dra*NADS to other NADS proteins suggest that the *dra*NADS seems to prefer NaAD as a substrate to synthesize NAD^+. In addition, our structural data can provide an idea related in ammonia detection through further research on biochemical mechanism of the *dra*NADS.

References

1. Foster, J. W.; Moat, A. G. *Microbiol. Rev.* **1980**, *44*, 83-105.
2. Begley, T. P.; Kinsland, C.; Mehl, R. A.; Osterman, A.; Dorrestein, P. *Vitam Horm.* **2001**, *61*, 103-119.
3. Belenky, P.; Bogan, K. L.; Brenner, C. *Trends Biochem. Sci.* **2007**, *32*, 12-19.
4. Battye, T. G.; Kontogiannis, L.; Johnson, O.; Powell, H. R.; Leslie, A. G. *Acta Crystallogr. D Biol. Crystallogr.* **2011**, *67*, 271-281.
5. Rizzi, M.; Nessi, C.; Mattevi, A.; Coda, A.; Bolognesi, M.; Galizzi, A. *EMBO J.* **1996**, *15*, 5125-5134.
6. Jauch, R.; Humm, A.; Huber, R.; Wahl, M. C. *J. Biol. Chem.* **2005**, *280*, 15131-15140.
7. McDonald, H. M.; Pruett, P. S.; Deivanayagam, C.; Protasevich, II; Carson, W. M.; DeLucas, L. J.; Brouillette, W. J.; Brouillette, C. G. *Acta Crystallogr. D Biol. Crystallogr.* **2007**, *63*, 891-905.
8. Kang, G. B.; Kim, Y. S.; Im, Y. J.; Rho, S. H.; Lee, J. H.; Eom, S. H. *Proteins* **2005**, *58*, 985-988.
9. Sorci, L.; Martynowski, D.; Rodionov, D. A.; Eyobo, Y.; Zogaj, X.; Klose, K. E.; Nikolaev, E. V.; Magni, G.; Zhang, H.; Osterman, A. L. *Proc. Natl. Acad Sci. USA* **2009**, *106*, 3083-3088.
10. Leslie, A. *Acta Crystallogr. D Biol. Crystallog.* **2006**, *62*, 48-57.
11. McCoy, A. J.; Grosse-Kunstleve, R. W.; Adams, P. D.; Winn, M. D.; Storoni, L. C.; Read, R. J. *J. Appl. Crystallogr.* **2007**, *40*, 658-674.
12. Emsley, P.; Cowtan, K. *Acta Crystallogr. D Biol. Crystallogr.* **2004**, *60*, 2126-2132.
13. Adams, P. D.; Afonine, P. V.; Bunkoczi, G.; Chen, V. B.; Davis, I. W.; Echols, N.; Headd, J. J.; Hung, L. W.; Kapral, G. J.; Grosse-Kunstleve, R. W.; McCoy, A. J.; Moriarty, N. W.; Oeffner, R.; Read, R. J.; Richardson, D. C.; Richardson, J. S.; Terwilliger, T. C.; Zwart, P. H. *Acta Crystallogr. D Biol. Crystallogr.* **2010**, *66*, 213-221.
14. Chen, V. B.; Arendall, W. B., 3rd; Headd, J. J.; Keedy, D. A.; Immormino, R. M.; Kapral, G. J.; Murray, L. W.; Richardson, J. S.; Richardson, D. C. *Acta Crystallogr. D Biol. Crystallogr.* **2010**, *66*, 12-21.